Springer

KSME

Journal of Mechanical Science and Technology 32 (10) (2018) 4829~4838
www.springerlink.com/content/1738-494x(Print)/1976-3824(Online)
DOI 10.1007/s12206-018-0930-1

Investigation on the semi-conjugate tooth model and disc milling process of logarithmic spiral bevel gears of pure-rolling contact †

Rulong Tan[1,2], Changyan Peng[1] and Bingkui Chen[1,*]

[1]*State Key Laboratory of Mechanical Transmission, Chongqing University, Chongqing, China*
[2]*College of Electrical Engineering, Chongqing University, Chongqing, China*

(Manuscript Received December 15, 2017; Revised May 29, 2018; Accepted July 1, 2018)

Abstract

Conventional logarithmic spiral bevel gears (LSBGs) introduce full-conjugate surfaces (line contact) to generate teeth of the pinion and the gear. However, in general, these full-conjugate surfaces are constructed by spherical involute curves and it is difficult to manufacture these surfaces. Therefore, this article tries to use semi-conjugate surfaces (point contact) as the tooth profiles to make they can be manufactured by the disc milling process and of pure-rolling contact. The design method, manufacture kinematics and stress distribution situations of the LSBGs with semi-conjugate surfaces are investigated. Conjugate surface theory and spatial conjugate curve meshing theory are both introduced to complete the analytical arguments. Finite element analysis (FEA) is introduced to evaluate the contact mechanical characteristics of the LSBGs under loads. From the analytical and simulated results, it is concluded that, through the disc milling process, the LSBGs of continuous pure-rolling contact can be manufactured and mesh correctly. Besides, the manufactured LSBGs maintain pure-rolling contact approximately when they are under loads.

Keywords: Logarithmic spiral bevel gears; Manufacture kinematics; Contact mechanics; Point contact; Pure-rolling contact

1. Introduction

Spiral bevel gears are widely used in the power transmission mechanism like vehicle axle, helicopter rotor reducer, etc. From the classic conjugate surface theory, much valuable research has been presented. Wildhaber and Baxter [1, 2] develop the initial theory of designing and analyzing bevel gears including local synthesis method. Tsai and Chin [3] investigate the tooth geometrical models of straight bevel gears and spiral bevel gears. Fan [4] describes the geometry of the face-milling and face-hobbing spiral bevel gears. Gonzalez-Perez and Fuentes-Aznar [5] investigate the kinematic conditions of face-hobbing spiral bevel gears and developed an analytical approach to determinate the machine-tool settings of these gears. Simon [6, 7] proposes a method of minimizing tooth contact pressures and angular displacement errors by optimizing head-cutter geometry and machine tool settings. Although the face milling and face hobbing spiral bevel gears are used most widely, due that the composite manufacture motions of the face milling and face hobbing processes is easy to be completed on the pure-mechanical machining tools, the two type of spiral bevel gears also have some defects such like, excessive relative sliding at the heel and toe of the tooth, erratic force directions of tooth surfaces, etc.

As for the conventional spiral bevel gears, the excessive relative sliding at the heel and toe of the tooth means serious sliding contact which has a more negative influence on the performance of gears compared to the rolling contact, because it could induce more serious frictional loss, adhesive wear, pitting, etc [8-10]. So, recently, researchers start to develop the gear geometry of continuous pure-rolling contact, which means sliding contact would not happen in the meshing cycle [11-14]. However, the research mainly concentrates on the field of cylindrical gears. In the other side, on account of the erratic force direction problem of conventional spiral bevel gears, Huston and Coy [15, 16] argue and compare the geometric kinematics of conventional spiral bevel gears and LSBGs which employ true spherical involute profile in theory. At last, they conclude that LSBGs can have better performance without regard to their manufacture convenience. Xiang et al. [17] investigate the variations of the output angular velocity and contact force of logarithmic spiral bevel gears and draw a similar conclusion. Subsequently, Duan et al. [18] propose a type of LSBG whose normal section profile is designed like that of Wildhaber-Novikov gear. Further, Alves et al. [19] investigates the manufacture method of LSBGs which employ spherical involutes as tooth surfaces by 5-axis com-

*Corresponding author. Tel.: +86 23 65106247, Fax.: +86 23 65106247
E-mail address: bingkui@cqu.edu.cn
† Recommended by Associate Editor Yongho Jeon

puter numerical control (CNC) milling machines. Recently, Xiang et al. [20] study the accurate modeling method of LSBGs and manufactured a prototype gear on the 5-axis CNC machine tool. Although the LSBGs have been manufactured by CNC milling machines in present studies, their manufacture efficiency is relatively lower because ball end cutters and multi-axis CNC milling machines are necessary for manufacturing the complex spherical involute helicoid.

A main reason which makes the LSBGs difficult to be manufactured is that, conventional LSBGs introduce full-conjugate surfaces (line contact) to generate teeth. These full-conjugate surfaces are usually spherical involute helicoids which hardly can be generated by disc milling cutters and several simple translation and rotation motions. However, in the gear transmission field, full-conjugate surfaces are not necessary for designing tooth profiles. In fact, semi-conjugate surfaces (point contact) are used more widely in practical bevel gear transmission mechanism [21]. In the other side, Chen et al. [22-24] propose the theory of spatial conjugate curve meshing. From the theory of spatial conjugate curve meshing, the tooth profiles of gears are semi-conjugate surfaces naturally.

This article aims to develop the theory of semi-conjugate LSBGs to make the LSBGs can be manufactured by the disc milling process, which have higher manufacture efficiency than the ball milling process. In the other side, from spatial conjugate curve meshing theory, the contact points can be always on the pitch line, so this article also tries to make the LSBGs of pure-rolling contact. In this article, the kinematic geometry of LSBGs of pure rolling contact is investigated first by introducing both spatial conjugate curve meshing theory first. Then the manufacture principles of LSBGs of pure rolling contact by disc milling process are investigated based on conjugate surface theory. At last, a numerical example is put forward to evaluate the contact mechanical characteristics of the proposed semi-conjugate LSBGs.

2. Geometry of LSBGs

2.1 Applied coordinate systems

Coordinate systems in the meshing process of spiral bevels are shown in Fig. 1. Coordinate systems S_0 and S_p are fixed in the absolute space. Movable coordinate systems S_1 and S_2 are attached to the pinion and gear, respectively. In this article, the kinematic conditions of the pinion and gear are set as below: The pinion and the gear only rotate about z_0 and z_p, respectively; the shaft angle ξ between the two revolving axles is invariant; the velocity ratio between the pinion and gear, i_{21}, is a constant. In Fig. 2, φ and ψ denote the rotational angle of the pinion and that of the gear respectively. ψ can be represented by φ and i_{21} through the equation $\phi = i_{21}\varphi$.

2.2 Spatial conjugate curve

From spatial conjugate meshing theory, an arbitrary space

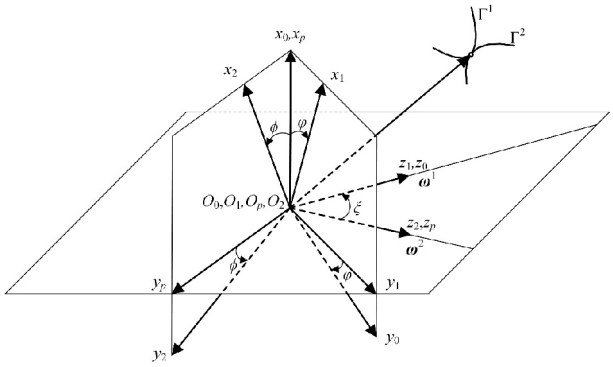

Fig. 1. Applied coordinate systems.

regular curve denoted as Γ^1, can be chosen as the contact path of the pinion. Then, from the designed contact directions along Γ^1 and meshing condition, its conjugate curve denoted as Γ^2 can be derived.

Based on the gearing kinematics [25], the relative velocity of the gears can be represented:

$$\boldsymbol{v}_0^{12}(\varphi,t) = \boldsymbol{\omega}_0^1 \times \boldsymbol{r}_0^1(\varphi,t) - \boldsymbol{\omega}_0^2 \times \boldsymbol{r}_0^1(\varphi,t) \tag{1}$$

where $\boldsymbol{\omega}^1$ represents the angular velocity vector of the pinion and $\boldsymbol{\omega}^2$ represents that of the gear. Besides, the subscript "i" of the vector notations indicates the representations of the vectors in "S_i".

In S_1, this relative velocity can be obtained by direct coordinate transform:

$$\boldsymbol{v}_1^{12}(\varphi,t) = \boldsymbol{M}_{10}(\varphi)\boldsymbol{v}_0^{12}(\varphi,t)\,. \tag{2}$$

From gear meshing theory, meshing equation is the necessary condition of meshing correctly. In other word, in gear tooth surface design, this equation need be true:

$$\boldsymbol{n}(t) \bullet \boldsymbol{v}^{12}(\varphi,t) = 0\,. \tag{3}$$

Here, $\boldsymbol{n}$ is the normal vector of the surface at a point on the tooth surface. As for the gears based on conjugate surface theory, $\boldsymbol{n}$ is the normal vector of the tooth surface. It determines the contact direction between a pair of conjugate surfaces. Similarly, from the idea of spatial curve meshing, an arbitrary normal vector of Γ^1, $\boldsymbol{n}$, can also be set as the contact direction between a pair of spatial curves.

In the theory of the surface geometry, if the tooth surface is determined, its normal vector $\boldsymbol{n}$ is exclusive which is determined by the surface geometry. However, for the spatial curve, $\boldsymbol{n}$ can be an arbitrary normal vector of Γ^1. Even if Γ^1 is determined, its normal vector $\boldsymbol{n}$ is not exclusive and the contact direction is also not exclusive at a point on Γ^1. So, to make the contact direction exclusive, the normal vector (contact direction) along Γ^1 can be set as a continuously differentiable vector function. Its general equation is represented as:

$$\boldsymbol{n}_1(t)=\cos\theta_1(t)\boldsymbol{\beta}_1^1(t)+\sin\theta_1(t)\boldsymbol{\gamma}_1^1(t)\,. \tag{4}$$

In Eq. (4), $\boldsymbol{\beta}_1^1$ represents the principal normal vector of Γ^1 and $\boldsymbol{\gamma}_1^1$ represents its binormal vector in S_1. Besides, θ_1 refers to the intersection angle between $\boldsymbol{n}$ and $\boldsymbol{\beta}^1$, which rotates counterclockwise about $\boldsymbol{\alpha}^1$. θ_1 represents a continuously differentiable function about the curve parameter t. It can be found that from Eq. (4) there is only one normal vector of Γ^1 at a point.

In S_2, the locus of Γ^1 can be derived by coordinate transformation:

$$\boldsymbol{r}_2^2(t,\varphi)=\boldsymbol{M}_{2p}\boldsymbol{M}_{p0}\boldsymbol{M}_{01}\boldsymbol{r}_1^1=\boldsymbol{M}_{21}\boldsymbol{r}_1^1\,. \tag{5}$$

Then, according to Ref. [23], the mathematical representations of spatial conjugate curve Γ^2 in S_2 can be obtained from Eqs. (3) and (5):

$$\begin{cases}\boldsymbol{n}_1(t)\bullet\boldsymbol{v}_1^{12}(\varphi,t)=0\\ \boldsymbol{r}_2^2(t,\varphi)=\boldsymbol{M}_{21}\boldsymbol{r}_1^1\,.\end{cases} \tag{6}$$

Eq. (6) represents a spatial curve, this spatial curve is the conjugate curve of Γ^1. It should be noted that the contact direction is $\boldsymbol{n}_1$, so the relative velocity between the pair of spatial conjugate curves is equal to zero only in the direction of $\boldsymbol{n}_1$ at a contact point.

2.3 Semi-conjugate tooth surface model

From a pair of spatial conjugate curves, the semi-conjugate surfaces can be generated. To make the semi-conjugate surfaces can inherit the contact characteristics of the spatial conjugate curves such like contact directions, contact paths, two conditions are necessary. First, a semi-conjugate surface must contain corresponding spatial conjugate curve. Second, the normal vectors of the semi-conjugate surfaces must be the same as $\boldsymbol{n}_1$ at corresponding point. Based on the two conditions above, the semi-conjugate tooth surface can be represented as a series of continuously variable plane curves named Γ^{s1} on the normal plane of Γ^1 as Fig. 2 shows. At each intersection point between Γ^{s1} and Γ^1, the principal normal vector of Γ^{s1} should the same as Eq. (4) determines. Then, the normal vector of tooth surface constructed by the curve set of Γ^{s1} will be the same as Eq. (4) represents along Γ^1. At last, by the local coordinate systems on Γ^1, this tooth surface can be represented in math.

At any point of Γ^1, $\boldsymbol{\alpha}^1$, $\boldsymbol{n}$ and $\boldsymbol{\alpha}^1$, $\boldsymbol{\alpha}^1\times\boldsymbol{n}$ construct a Cartesian coordinate system notated as S_{1Fr}. Then, in S_{1Fr}, arbitrary Γ^{s1} could be represented in this form:

$$\boldsymbol{r}_{Fr1}^{sec1}(u)=(0\quad y(u)\quad z(u)\quad 1)^{\mathrm{Tr}}\,. \tag{7}$$

Therefore, through coordinate transforming, Σ^1 in S_1 is represented:

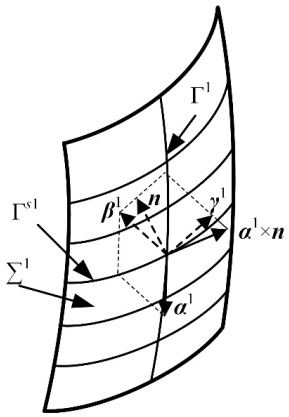

Fig. 2. Tooth surface schematic from Γ^1 and Γ^{s1}.

$$\boldsymbol{S}_1^1(t,u)=\boldsymbol{M}_{1Fr1}(t)\boldsymbol{r}_{Fr1}^{sec1}(u) \tag{8}$$

where

$$\boldsymbol{M}_{1Fr1}(t)=\begin{pmatrix}\boldsymbol{i}_1^1\bullet\boldsymbol{\alpha}_1^1 & \boldsymbol{i}_1^1\bullet\boldsymbol{n}_1 & \left(\boldsymbol{i}_1^1,\boldsymbol{\alpha}_1^1,\boldsymbol{n}_1\right) & \\ \boldsymbol{j}_1^1\bullet\boldsymbol{\alpha}_1^1 & \boldsymbol{j}_1^1\bullet\boldsymbol{n}_1 & \left(\boldsymbol{j}_1^1,\boldsymbol{\alpha}_1^1,\boldsymbol{n}_1\right) & \boldsymbol{r}_1^1\\ \boldsymbol{k}_1^1\bullet\boldsymbol{\alpha}_1^1 & \boldsymbol{k}_1^1\bullet\boldsymbol{n}_1 & \left(\boldsymbol{k}_1^1,\boldsymbol{\alpha}_1^1,\boldsymbol{n}_1\right) & \\ 0 & 0 & 0 & \end{pmatrix}. \tag{9}$$

Here, the bracket denote the mixed product of the three vectors in it, for example, $\left(\boldsymbol{i}_1^1,\boldsymbol{\alpha}_1^1,\boldsymbol{n}_1\right)=\boldsymbol{i}_1^1\bullet\left(\boldsymbol{\alpha}_1^1\times\boldsymbol{n}_1\right)$.

The process of generating Σ^2 from Γ^2 and Γ^{s2} is the same as that of Σ^1 in S_1. On consideration that meshing equation is true only along the spatial conjugate curves, when a pair of these tooth surfaces mesh, only the points on Γ^1 and Γ^2 satisfy the laws of gear meshing. In other words, these tooth surfaces are of point contact and the contact point only moves along Γ^1 and Γ^2, respectively. These tooth surfaces are semi-conjugate.

2.4 Continuous pure-rolling contact condition

The pure-rolling contact means at the contact point, the magnitude of the relative velocity is equal to zero, which means:

$$\boldsymbol{v}_1^{12}=\boldsymbol{0}. \tag{10}$$

For spiral bevel gears, only when the contact point locates at the pitch cone, Eq. (10) might be true. From above arguments about semi-conjugate surfaces, Γ^1 and Γ^2 represent the contact paths of the pinion and the gear. Therefore, to make bevel gears pure-rolling contact, Γ^1 should be a regular curve on the pitch cone. The pitch cone can be described as:

$$\boldsymbol{S}_1^1(t,u)=\left(up\sin(t)\quad up\cos(t)\quad u\quad 1\right)^{\mathrm{Tr}}. \tag{11}$$

Here $p=\tan(\delta)$ and δ is pitch cone angle of the pinion and t

is the basic circle parameter as Fig. 3 shows.

Then, from Eq. (11), ordering $u = f(t)$, an arbitrary conical spiral, Γ^1, can be represented:

$$\begin{aligned} \boldsymbol{r}_1^1(t) &= \boldsymbol{S}_1^1(t, f(t)) \\ &= \begin{pmatrix} pf(t)\sin(t) & pf(t)\cos(t) & f(t) & 1 \end{pmatrix}^{\mathrm{Tr}}. \end{aligned} \tag{12}$$

Synthesizing Eqs. (3) and (10), it can be observed Eq. (10) makes meshing equation true naturally.

In the other hand, from Eq. (1), the relative velocity is derived in S_1:

$$\boldsymbol{v}_1^{12} = \begin{pmatrix} f(t)\left(p\cos t\left(i_{21}\cos\xi - 1\right) - i_{21}\sin\xi\cos\varphi\right) \\ f(t)\left(i_{21}\sin\xi\sin\varphi + \sin t\left(p - i_{21}p\cos\xi\right)\right) \\ i_{21}pf(t)\sin\xi\sin(t-\varphi) \\ 0 \end{pmatrix}. \tag{13}$$

After Eq. (13) is substituted into Eq. (10), the condition of pure-rolling contact is derived:

$$\begin{cases} t = \varphi \\ p = \dfrac{i_{21}\sin\xi}{-1 + i_{21}\cos\xi}. \end{cases} \tag{14}$$

Then, from Eqs. (5) and (14), the spatial conjugate curve Γ^2 of Γ^1 is obtained:

$$\begin{aligned} \boldsymbol{r}_2^2(t) &= \boldsymbol{M}_{21}(t)\boldsymbol{r}_1^1(t) \\ &= \begin{pmatrix} f(t)\sin\left(i_{21}t\right)(p\cos\xi - \sin\xi) \\ f(t)\cos\left(i_{21}t\right)(p\cos\xi - \sin\xi) \\ f(t)(\cos\xi + p\sin\xi) \\ 1 \end{pmatrix}. \end{aligned} \tag{15}$$

Just from previous derivations of this section, it can be found that the function $f(t)$ is not restricted. Therefore, Γ^1 can be an arbitrary regular curve on the pitch cone. So, a conical helix of the pitch cone can be set as Γ^1. In the other hand, Γ^1 is also the tooth trace of generated bevel gears (Γ^1 is the intersection curve between the tooth surface and the pitch cone), so LSBG can be generated based on spatial curve meshing theory from Γ^1.

2.5 Mathematical model of conical helixes

As for the LSBG, the key geometric characteristic is that its tooth line is a conical helix. For a conical helix, the intersection angle between its tangent vector and the basic cone generator at any point keep constant which means the magnitudes of β_k keep constant (see Fig. 3). To make the semi-conjugate tooth surfaces of the LSBGs satisfy the continuous pure-rolling contact condition, a conical helix on the pitch cone of the pinion is set as Γ^1. It can be represented by the equations:

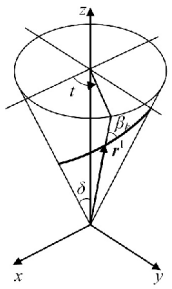

Fig. 3. Diagram of an arbitrary conical spiral.

$$\boldsymbol{r}_1^1(t) = \begin{pmatrix} ne^{mt}\sin(t) & ne^{mt}\cos(t) & be^{mt} & 1 \end{pmatrix}^{Tr} \tag{16}$$

where $n = \sin(\delta)$, $m = \sin(\delta)\cot(\beta_k)$, $b = \cos(\delta)$.

Comparing Eqs. (12) and (16), the function $f(t)$ is obtained:

$$\begin{cases} f(t) = be^{mt} \\ p = n/b. \end{cases} \tag{17}$$

After Eq. (17) are substituted into Eq. (15), the spatial conjugate curve of Γ^1, Γ^2 is obtained:

$$\boldsymbol{r}_2^2(t) = \begin{pmatrix} e^{mt}\sin\left(i_{21}t\right)(n\cos\xi - b\sin\xi) \\ e^{mt}\cos\left(i_{21}t\right)(n\cos\xi - b\sin\xi) \\ e^{mt}(b\cos\xi + n\sin\xi) \\ 1 \end{pmatrix}. \tag{18}$$

Observing Eq. (18), it can be found, Γ^2 is also the conical helix on the gear's pitch cone. Therefore, from Γ^2, another LSBG can be generated.

3. Manufacture method LSBGs by disc milling process

3.1 Manufacture coordinate systems

Applied coordinate systems are represented in Fig. 4 in the process of investigating the disc milling process. S_0 is fixed in the absolute space. S_1 is connected to the workpiece. S_m and S_c are connected to the milling tool. The original points of S_m and S_c, O_m and O_c locate at the same point P which is the intersection point between the pitch line and Γ^1. In S_m, y_m-axis share the same direction with the pitch line between the pinion and the gear. In S_c, y_c-axis share the same direction with the tangential direction of Γ^1. So the intersection angle between y_m-axis and y_c-axis is β_k. Besides, the direction of z_c-axis is the same with that of z_m-axis and it is perpendicular to the plane which is constructed by y_c-axis and y_m-axis. The tool revolving axis is in the z_c-x_c plane and the distance between tool

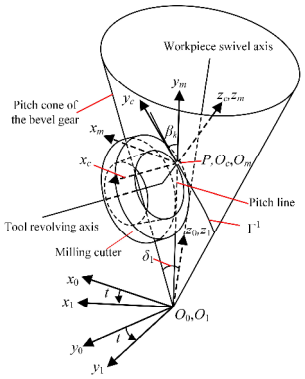

Fig. 4. Isometric project view of the disc milling process of LSBG.

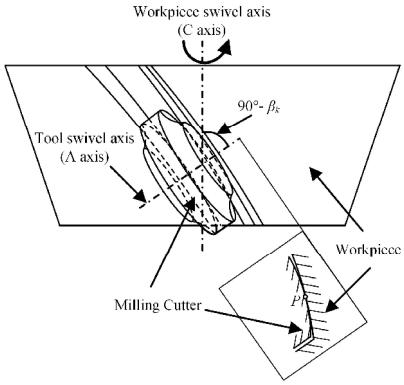

Fig. 5. Front view of the disc milling process of LSBG.

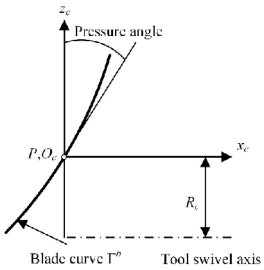

Fig. 6. Schematic of the blade.

revolving axis and x_c-axis is the difference between half the outer diameter of cutter and the dedendum of the gear, namely $d_{a0}/2$-h_{fm}. Then the velocity direction of the tool generating surface at P will be the same as y_c-axis. In the process of milling, S_m and S_c will move with the point P along the y_m-axis.

3.2 Kinematic model of disc milling process

From the arguments in Sec. 2, it can be found that for the manufactured LSBG of pure rolling contact, the necessary condition of meshing correctly is that the two designed conical helixes which are also spatial meshing curves, located on the manufactured tooth surfaces. On consideration that the pinion and the gear are both the LSBGs of pure rolling contact in Sec. 2, only the disc milling process of the pinion is descripted and that of the gear is similar.

To make the manufactured tooth surfaces contain the designed conical helixes, the kinematics conditions of the disc milling process are set: 1. The rotation angle of the pinion workpiece is the same as the basic circle angular parameter in Sec. 2, namely, t; 2. The intersection angle between the tool swivel axis and the workpiece swivel axis is 90°-β_k; 3. A linear movement of the tool exists and its direction is along the y_m-axis. The linear displacements of the milling cutter can be resolved into two components along y_0 axis and x_0 axis, respectively:

$$\begin{cases} U_{y0} = e^{mt}\sin\delta_1 \\ U_{z0} = e^{mt}\cos\delta_1 \end{cases}. \tag{19}$$

Then, on consideration that $n/b = i_{21} = p$, the locus of the point P on the generating surface of the milling cutter in S_1, will form the designed conical helix Γ^1.

$$\begin{aligned} \boldsymbol{r}_1^P &= \boldsymbol{M}_{1c}(t)(0 \quad 0 \quad 0 \quad 1)^{Tr} \\ &= \left(ne^{mt}\sin(t) \quad ne^{mt}\cos(t) \quad be^{mt} \quad 1\right)^{Tr}. \end{aligned} \tag{20}$$

Subsequently, it will be demonstrated that the locus of the point P of the milling cutter generating surface in S_1 is also on the manufactured tooth surface. Then, based on the arguments in Sec. 2.3, if the designed conical helixes are regarded as a pair of spatial conjugate curves, the manufactured tooth surfaces will satisfy the first condition of semi-conjugate surfaces which can inherit the contact characteristics of the conical helixes.

3.3 Tooth surfaces of manufactured gears

Based on the arguments in Sec. 2, it can be found that for the manufactured LSBG of pure rolling contact, a necessary condition of meshing correctly is that the two designed conical helixes which are also spatial meshing curves, located on the manufactured tooth surfaces.

From gearing theory, the tooth surface of the manufactured gear can be derived from conjugate surface theory [25]. We denote the blade of the tool as Γ^b and use the position vector $\boldsymbol{r}^b(u)$ to represent Γ^b just as Fig. 6 shows. Then, the generating surface of the milling cutter is produced by the locus of Γ^b in S_c. From Fig. 6, the tooth surface equation of the generating surface is obtained:

$$\boldsymbol{S}_c^g(\eta,u) = \begin{pmatrix} 1 & 0 & 0 & 0 \\ 0 & \cos(\eta) & -\sin(\eta) & 0 \\ 0 & \sin(\eta) & \cos(\eta) & 0 \\ 0 & 0 & 0 & 1 \end{pmatrix} \begin{pmatrix} 0 \\ 0 \\ R_c \\ 0 \end{pmatrix} + \boldsymbol{r}_c^b(u) - \begin{pmatrix} 0 \\ 0 \\ R_c \\ 0 \end{pmatrix} \tag{21}$$

where η refers to the rotation angle of Γ^b from the original

location about the tool swivel axis and u refers to the curve parameter of Γ^b. Here, let the position vector of P in S_c is that:

$$\boldsymbol{S}_c^g(0,0)=(0 \quad 0 \quad 0 \quad 1)^{Tr}. \tag{22}$$

Then, the locus of the generating surface of the milling cutter in S_1 is obtained:

$$\boldsymbol{S}_1^g(t,\eta,u)=\boldsymbol{M}_{1c}(t)\boldsymbol{S}_c^g(\eta,u). \tag{23}$$

From Eq. (23), the relative velocity between the generating surface and manufactured gear is derived:

$$\boldsymbol{v}_c^{1g}(t,\eta,u)=t'\boldsymbol{M}_{c1}(t)\frac{\mathrm{d}\boldsymbol{M}_{1cr}(t)}{\mathrm{d}\varphi}\boldsymbol{S}_c^g(\eta,u) \tag{24}$$

where the notation t' refers to time derivative of t.

At P, synthesizing Eqs. (22) and (24), the relative velocity is obtained:

$$\begin{aligned}\boldsymbol{v}_c^{1gP}&=t'\boldsymbol{M}_{c1}(t)\frac{\mathrm{d}\boldsymbol{M}_{1c}(t)}{\mathrm{d}t}(0 \quad 0 \quad 0 \quad 1)^{Tr}\\&=t'ne^{mt}\begin{pmatrix}\dfrac{i_{21}\cos\beta_k}{\sqrt{i_{21}{}^2+(i_{21}\cot\xi-\csc\xi)^2}}+m\sin\beta_k\\ m\cos\beta_k-\dfrac{i_{21}\sin\beta_k}{\sqrt{i_{21}{}^2+(i_{21}\cot\xi-\csc\xi)^2}}\\0\\0\end{pmatrix}.\end{aligned} \tag{25}$$

On consideration that $m=\sin(\delta)\cot(\beta_k)$ p = $\tan(\delta)$ and Eqs. (4) and (25) will be simplified as:

$$\boldsymbol{v}_c^{1gP}=t'ne^{mt}\left(0 \quad \cot\beta_k\cos\beta_k+\sin\beta_k\sin\delta \quad 0 \quad 0\right)^{Tr}. \tag{26}$$

As for the generating surface, its normal vector in S_1 is represented as:

$$\boldsymbol{n}_1^g(t,\eta,u)=\boldsymbol{M}_{1c}(t)\left(\frac{\partial\boldsymbol{S}_c^g(\eta,u)}{\partial\eta}\times\frac{\partial\boldsymbol{S}_c^g(\eta,u)}{\partial u}\right). \tag{27}$$

Because the normal vectors on the surface of the milling cutter point to the tool swivel axis, the normal vector at P can be represented as:

$$\boldsymbol{n}_c^{gP}=\left(n_c^{gP} \quad 0 \quad n_c^{gP} \quad 0\right)^{Tr}. \tag{28}$$

From Eqs. (24) and (27), the meshing equation between the generating surface and the manufactured gear is represented:

$$f(t,\eta,u)=\boldsymbol{n}_1^g\bullet\boldsymbol{v}_1^{1g}=\boldsymbol{n}_c^g\bullet\boldsymbol{v}_c^{1g}=0. \tag{29}$$

From the conjugate surface theory, the manufactured gear tooth surface by the generating surface can be obtained from Eqs. (23) and (29). Namely, the mathematical representation of the manufactured tooth surface is:

$$\begin{cases}\boldsymbol{S}_1^g(t,\eta,u)=\boldsymbol{M}_{1c}(t)\boldsymbol{S}_c^g(\eta,u)\\ f(t,\eta,u)=0.\end{cases} \tag{30}$$

At P, from Eqs. (26) and (28), it can be observed that the meshing equation between the workpiece and the milling cutter at P is always true:

$$f(t,0,0)=\boldsymbol{n}^{gP}\bullet\boldsymbol{v}^{g1c}=\boldsymbol{n}_c^{gP}\bullet\boldsymbol{v}_c^{g1c}=0. \tag{31}$$

Therefore, from Eqs. (30) and (31), it can be indicated that $\boldsymbol{S}_1^g(t,0,0)$ is a curve on the manufactured tooth surface, this curve can be represented as:

$$\begin{aligned}\boldsymbol{S}_1^g(t,0,0)&=\boldsymbol{M}_{1c}(t)\boldsymbol{S}_c^g(0,0)\\&=\left(ne^{mt}\sin(t) \quad ne^{mt}\cos(t) \quad be^{mt} \quad 1\right)^{Tr}.\end{aligned} \tag{32}$$

It can be found that Eqs. (16), (20) and (32) represent the same curve. Therefore, it is concluded that through disc milling processing with proposed associated linear motion and revolving motion, the designed conical helix can be contained on the manufactured tooth surface.

3.4 Tool geometry

In Sec. 3.3, the first necessary condition of semi-conjugate surfaces has been demonstrated that it can be satisfied by disc milling process. Then from Sec. 2.3, second necessary condition of semi-conjugate is that the normal vectors of the semi-conjugate surface must be the same as the designed contact direction at corresponding point.

From gearing theory, at P, the normal vector of a manufactured tooth surface is the same with that of corresponding generating surface of the milling cutter. So, a method that make second necessary condition true is that let the two generating surfaces be tangent at P and their common normal vector be $\boldsymbol{n}^{gP}$ at P. On consideration that $\boldsymbol{n}^{gP}$ is on the z_c-x_c plane, which is also the normal plane of Γ^1 just as Fig. 4 shows, $\boldsymbol{n}^{gP}$ can be regarded as the designed contact direction in Sec. 2.2. Then, the normal vectors of the manufactured tooth surfaces are the same as $\boldsymbol{n}^{gP}$ at P. The second condition is satisfied.

Then according to the geometry of formatting milling cutters of involute gears, the disc milling cutter can be designed as Fig. 8 shows.

To make the two generating surfaces be tangent at P and their common normal vector be $\boldsymbol{n}^{gP}$ at P, the profile curves of the blade can be designed to be tangent at P and their principal normal vectors are in the same direction with $\boldsymbol{n}^{gP}$. Here, the

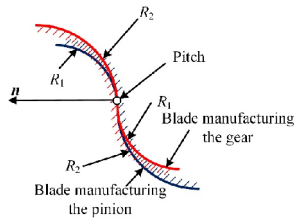

Fig. 7. The geometry of blades.

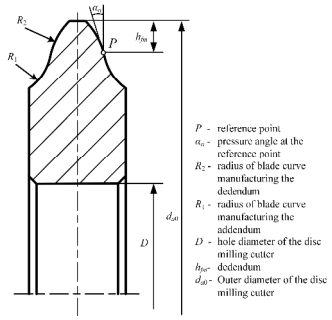

Fig. 8. Shape of the disc milling cutter.

profiles of the blade with double-arc curves are proposed just as Fig. 7 shows. There are several reasons that introduce this double-arc curve as the profile of a blade in this article. First, due to the difference of the curvatures of the two curve on the blade, the contact point can be easily controlled on the pitch line. Second, the concave curves at the dedendum part can enlarge the thickness of gear teeth at roots, so this shape of a cross-section curve contributes to decrease- the bending stress of gears. At last, this profile makes the blades manufacturing the pinion or gear have the same shapes, so one cutter can be used to manufacture both the pinion and gear.

3.5 Example

Based on previous arguments, the tooth surfaces of LSBGs of continuous pure-rolling contact can be obtained. The geometrical parameters of the pinion and the gear are set as Table 1. The arc radius of the blades are set as, R_1 = 6 mm, R_2 = 10 mm. The mainly geometrical parameters of the pinion and the gear are shown in Table 2. Then, from the disc milling processing model in section 3, the tooth surfaces of manufactured gears are obtained (see Fig. 9).

4. Loaded tooth contact analysis

In this section, the loaded tooth contact analysis of the manufactured LSBGs in Sec. 3 is completed by finite element analysis. Through this analysis, the mechanical characteristics of the LSBG are evaluated.

From the solid model as Fig. 9 shows, a 3-pair-of-teeth finite element model is built (see Fig. 10). In this model, first eight-node order elements, whose max length size is set as 2 mm, are used to generate the finite element model. Flexible

Table 1. Geometrical parameters for a pair of LSBGs.

Terms	Pinion	Gear
Number of teeth	8	24
Spiral angle	35°	35°
Pitch angle	18.435°	71.565°
Addendum	1.8 mm	1.8 mm
Dedendum	2.8 mm	2.8 mm
Outside pitch diameter	54 mm	162 mm
Hand of spiral	LH	RH
Face width	30 mm	
gear ratio	1:3	
Shaft angle	90°	
Pressure angle	20°	

Table 2. Geometrical parameters for the disc cutter.

Terms	Magnitudes
Pressure angle	20°
Radius of blade curve	R_1 = 6 mm, R_2 = 10 mm
Outer diameter	105 mm

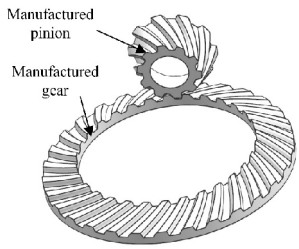

Fig. 9. Assemble model of the manufactured pinion and gear.

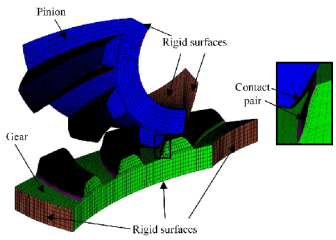

Fig. 10. Finite element model.

surface-to-surface contact elements are superposed on the tooth surfaces. On consideration of the intensive stress variations, the max length size of the elements attached to tooth surfaces is set as 0.2 mm. To apply rotation and torque on the pinion and the gear, two pairs of rigid surfaces are built as Fig. 10 shows. The material is set as gear steel whose Young's Modulus is 2.05×10^5 MPa and Poisson's ratio 0.3. Then, after the calculations of the solver for the finite element model, the stress distributions about these spiral bevel gears under loads are obtained.

Fig. 11 shows the stress distributions when the contact point

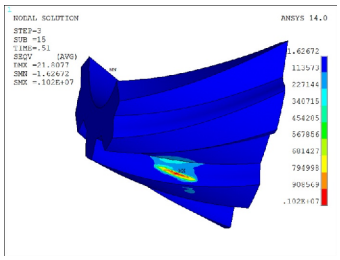

Fig. 11. Stress distributions of the pinion in the mesh cycle.

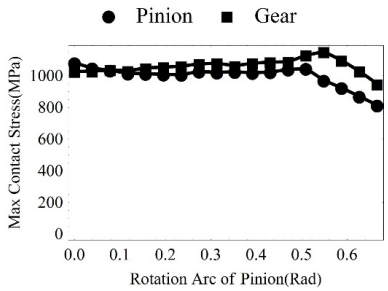

Fig. 12. Max contact stresses of the gears on the middle tooth.

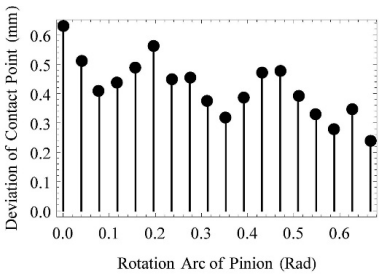

Fig. 13. The deviation distance between theoretical and real locations with max contact pressure.

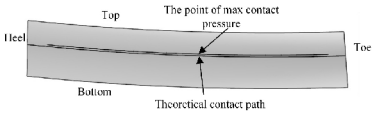

Fig. 14. Theoretical contact path and real contact path on the tooth surface.

located at the center of the middle tooth surface. Based on Hertz contact theory, the contact pattern of theoretical contact point expands to an ellipse due to the elastic deformation of the tooth. Fig. 12 shows the variations of max contact stresses on the central pair of teeth in a meshing cycle. It can be observed the magnitude of the max contact stress varies smoothly and its maximum is 1100 MPa. This situation means that for this LSBG, no serious stress concentration such like edge contact stress concentration occurred.

In Hertz theory, the max contact pressure should locate at the theoretical contact point for two elastic solids under loads. Figs. 13 and 14 show these deviations of max contact pressure points in Hertz theory and FEA results. The deviations can be

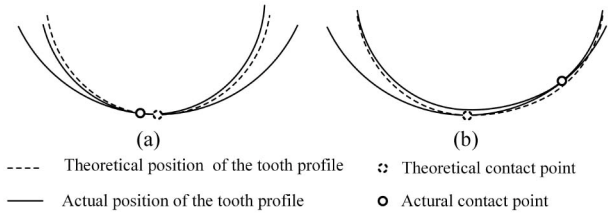

Fig. 15. The position deviations of contact point that are induced by (a) elastic deformation; (b) curvature interference.

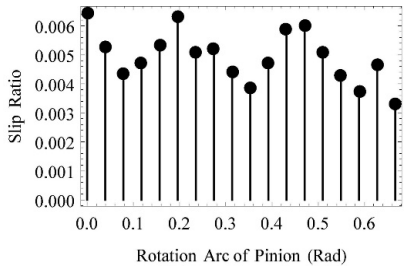

Fig. 16. Slip ratio at the points with max contact pressure.

interpreted by the two factors: First, in Hertz contact model, the influence of tooth bending deformations on the tooth surface geometry is not introduced; second, the continuous geometric models are converted into discrete models in the process of FEA. Due that the magnitudes of the deviations of max contact pressure points in Hertz theory and FEA results are small (less than 0.62 mm), these errors can be attributed to the influence of elastic deformations of teeth and deviations between continuum elastic model and finite element model. Because that interference usually can induce large deviations of the positions of the contact points from theoretical locations (see Fig. 15), it is concluded that the pinion and gear in Sec. 3 mesh correctly and no interference exists between them. Because these teeth of the pinion and the gear are generated by the same disc milling cutter with double-arc blades, it is also concluded that the double-arc curve can be used as the profile of the blade and both the pinion and the gear of LSBGs can be manufactured by one cutter with double-arc blade. What's more, from the results of FEA, based on the calculated contact points with max contact stresses, the slip ratios between the pinion and gear at the real max contact pressure point can also been derived. Fig. 16 shows the slip ratios between the pinion and gear at the real max contact pressure points. It can be found their magnitudes are still small as the maximum is 0.0063 which means the pinion and the gear are still of approximate pure-rolling contact.

5. Conclusions

From conjugate surface theory and spatial conjugate curve theory, the disc milling processing model of LSBGs of continuous pure-rolling contact is argued in this paper. Besides, based on these arguments, a pair of manufactured LSBGs

have been built and FEA is applied for them. From the arguments and FEA results, following conclusions can be drawn:

(1) The LSBGs of continuous pure-rolling contact can be manufactured by proposed disc milling process. The manufactured pinion and gear can mesh correctly and no interference exists between them.

(2) The disc milling processing can be completed by a revolving motion of the workpiece and corresponding translational motion of the cutter. So the minimum of linkage axis can be reduced to two.

(3) The double-arc curve can be used as the profile of the blade. When this shape of blade curve is used, both the pinion and the gear of LSBGs can be manufactured by one cutter.

(4) When a pair of the LSBGs meshing under loads, although the deviations between the theoretical and real points with max contact pressure exist, the magnitudes of the slip ratios are still small. So the pinion and the gear can be of approximate pure-rolling contact when they are under loads.

Acknowledgments

This research is supported by China Postdoctoral Science Foundation (Grant No.2017M612902), Chongqing Postdoctoral Science Foundation (Grant No. Xm2017108) and National Natural Science Foundation of China (Grant No. 51605049, 51575062). The authors of the paper express their deep gratitude to them for the financial support of research projects.

Nomenclature

E : (Effective) work potential
S_i : Coordinate systems fixed to tool ($i = c$, $i = m$), pinion ($i = 1$), gear ($i = 2$)
S_j : Coordinate systems fixed to absolute space corresponding to pinion ($j = 0$), gear ($j = p$), and tool ($i = c0$)
Γ^1 : The spatial contact curve on the pinion
Γ^2 : The spatial contact curve on the gear
Σ^i : Tooth surface ($i = 1$ for pinion and $i = 2$ for gear)
ξ : Shaft angle
φ : Pinion's revolving angle
$\boldsymbol{\varphi}$: Gear's revolving angle
η : Tool's revolving angle
δ : Cone angle
i_{21} : Gear ratio between the pinion and the gear
R_c : The turning radius of the milling cutter from the reference point P to its revival axis
$\boldsymbol{M}_{ij}$: Coordinate transformation matrix from S_j to S_i
$\boldsymbol{n}$: Common normal vector of Σ^1 and Σ^2 at contact position
r_i^j : Position vector of designed spatial curve($j = 1$) and corresponding spatial conjugate curve($j = 2$) in S_i
S_i^j : Position vector of tooth surface($j = 1$ for pinion and $i = 2$ for gear) in S_i

References

[1] E. Wildhaber, Surface curvature, *Product Engineering*, 27 (5) (1956) 184-191.
[2] M. L. Baxter, Second-order surface generation, *Industrial Mathematics*, 23 (2) (1973) 85-106.
[3] Y. C. Tsai and P. C. Chin, Surface geometry of straight and spiral bevel gears, *Journal of Mechanical Design*, 109 (4) (1987) 443-449.
[4] Q. Fan, Computerized modeling and simulation of spiral bevel and hypoid gears manufactured by gleason face hobbing process, *Journal of Mechanical Design*, 128 (6) (2005) 1315-1327.
[5] I. Gonzalez-Perez and A. Fuentes-Aznar, Analytical determination of basic machine-tool settings for generation of spiral bevel gears and compensation of errors of alignment in the cyclo-palloid system, *International Journal of Mechanical Sciences*, 120 (2017) 91-104.
[6] V. Simon, Design of face-hobbed spiral bevel gears with reduced maximum tooth contact pressure and transmission errors, *Chinese Journal of Aeronautics*, 26 (3) (2013) 777-790.
[7] V. V. Simon, Manufacture of optimized face-hobbed spiral bevel gears on computer numerical control hypoid generator, *Journal of Manufacturing Science and Engineering*, 136 (3) (2014) 031008.
[8] Y. Michlin and V. Myunster, Determination of power losses in gear transmissions with rolling and sliding friction incorporated, *Mechanism and Machine Theory*, 37 (2) (2002) 167-174.
[9] P. J. L. Fernandes and C. McDuling, Surface contact fatigue failures in gears, *Engineering Failure Analysis*, 4 (2) (1997) 99-107.
[10] M. Ristivojević, T. Lazović and A. Vencl, Studying the load carrying capacity of spur gear tooth flanks, *Mechanism and Machine Theory*, 59 (0) (2013) 125-137.
[11] M. J. Wagner, W. F. Ng and S. G. Dhande, Profile synthesis and kinematic analysis of pure rolling contact gears, *Journal of Mechanical Design*, 114 (2) (1992) 326-333.
[12] C.-H. Chen, A formula for determining limit noninterference curvature in pure rolling conjugation gears by using geometro-kinematical concepts, *Journal of Mechanical Design*, 117 (1) (1995) 180-184.
[13] Y. Song, Q. Liao, S. Wei, L. Guo, H. Song and L. Zhou, Modelling, simulation and experiment of a novel pure rolling cycloid reducer with involute teeth, *International Journal of Modelling, Identification and Control*, 21 (2) (2014) 184-192.
[14] R. Tan, B. Chen and C. Peng, General mathematical model of spiral bevel gears of continuous pure-rolling contact, *Proceedings of the Institution of Mechanical Engineers, Part C: Journal of Mechanical Engineering Science*, 229 (15) (2015) 2810-2826.
[15] R. L. Huston and J. J. Coy, Surface geometry of circular cut

spiral bevel gears, *Journal of Mechanical Design*, 104 (4) (1982) 743-748.

[16] R. L. Huston and J. J. Coy, Ideal spiral bevel gears—A new approach to surface geometry, *Journal of Mechanical Design*, 103 (1) (1981) 127-132.

[17] T. Xiang, L. Gu and J. Xu, The meshing angular velocity and tangential contact force simulation for logarithmic spiral bevel gear based on Hertz elastic contact theory, *Journal of Mechanical Science and Technology*, 30 (8) (2016) 3441-3452.

[18] Z. Duan, H. Chen, Z. Ju and J. Liu, Mathematical model and manufacture programming of loxodromic-type normal circular-arc spiral bevel gear, *Frontiers of Mechanical Engineering*, 7 (3) (2012) 312-321.

[19] J. T. Alves, M. Guingand and J.-P. de Vaujany, Designing and manufacturing spiral bevel gears using 5-axis computer numerical control (CNC) milling machines, *Journal of Mechanical Design*, 135 (2) (2013) 024502.

[20] T. Xiang, L. Gu and L. Xiao, Accurate modeling of logarithmic spiral bevel gear based on the tooth flank formation and Boolean addition operation, *Proceedings of the Institution of Mechanical Engineers, Part B: Journal of Engineering Manufacture*, 230 (9) (2016) 1650-1658.

[21] D. B. Dooner, *Kinematic geometry of gearing*, 2nd Edition, John Wiley & Sons Inc., New York, USA (2012).

[22] B. Chen, D. Liang and Z. Li, A study on geometry design of spiral bevel gears based on conjugate curves, *International Journal of Precision Engineering and Manufacturing*, 15 (3) (2014) 477-482.

[23] B. Chen, D. Liang and Y. Gao, Geometry design and mathematical model of a new kind of gear transmission with circular arc tooth profiles based on curve contact analysis, *Proceedings of the Institution of Mechanical Engineers, Part C: Journal of Mechanical Engineering Science*, 228 (17) (2014) 3200-3208.

[24] R. Tan, B. Chen, C. Peng and X. Li, Study on spatial curve meshing and its application for logarithmic spiral bevel gears, *Mechanism and Machine Theory*, 86 (2015) 172-190.

[25] F. L. Litvin and A. Fuentes, *Gear geometry and applied theory*, Cambridge University Press, New Jersey, USA (2004).

Rulong Tan received his doctor's degree in engineering from the State Key Laboratory of Mechanical Transmission, Chongqing University, China. Now, he is a postdoctoral fellow in Chongqing University. His research interests include bevel gear geometry, kinematics, and manufacturing.

Bingkui Chen is currently a Professor and Director for the State Key Lab of Mechanical Transmissions at Chongqing University, China. He is also Vice Director of the CMES Gear Technical Committee and a member of the CMES Gear Manufacturing Committee. Prof. Chen has conducted pioneering research related to gear geometry, kinematics, dynamics and manufacturing.